Theor Chem Acc (2006) 116: 514–523
DOI 10.1007/s00214-006-0089-1

REGULAR ARTICLE

E. Cottancin · G. Celep · J. Lermé · M. Pellarin
J.R. Huntzinger · J.L. Vialle · M. Broyer

Optical properties of noble metal clusters as a function of the size: comparison between experiments and a semi-quantal theory

Received: 8 January 2004 / Accepted: 11 May 2005 / Published online: 22 February 2006

Abstract The optical properties of noble metal clusters are measured and compared in the size range 1.4–7 nm in diameter. The clusters of copper, silver and gold are produced by the same experimental technique, the deposition of preformed clusters in a transparent matrix. The size dependence is found to be different for the three metals. As the size decreases, the surface plasmon resonance is only slightly blue-shifted for silver, more strongly blue-shifted and damped for gold while this peak resonance vanishes for copper. We show that these results cannot be interpreted by a simple classical theory. Since ab initio calculations are not possible in this size range, we obtain a complete theoretical description of these optical properties through the same semi-quantal model for the three metals.

Keywords Clusters · Metal nanoparticles · Optical properties · Surface plasmon resonance · Jellium · Time dependant local density approximation (TDLDA theory)

1 Introduction

The optical properties of metallic nanoparticles have fascinated scientists for a long time [1]. Recently, the progress in nanosciences have opened new fields of applications for these nanosystems, including near field sources [2], photonics integrated circuits [3] or biological labelling [4,5]. In this respect, the optical properties of noble metal nanoparticles are the most interesting because their UV–Visible absorption spectrum is dominated by a very intense resonance due to the collective motion of the *s*-valence electrons, the so-called surface plasmon resonance (SPR). Moreover, the nanoparticles of these materials are quite easy to handle in contrast with alkali, which are immediately oxidized in contact with air. Generally, in transition metal clusters, the optical properties are quite complicated to calculate and the SPR does not emerge because of the mixing of *s*- and *d*-bands due, for most of them, to open *d*-shells in the atom. On the contrary, in alkali clusters, the *s* electrons interact only weakly with the core electrons and the pure jellium model may be used to calculate the collective motion of *s* electrons. In recent years, it has been experimentally and theoretically demonstrated that the SPR emerges for size as small as eight atoms [6–8].

Noble metals atoms (Cu, Ag and Au) have closed shell *d* levels, but in the bulk the valence *d*-band and conduction *s*-band are still energetically close together. In clusters, the SPR emerges more or less easily depending on the metallic element, but it is strongly influenced by the *d* electrons. The simplest system is silver. The threshold for interband transitions in the bulk is quite high (around 4 eV). The SPR emerges for very small sizes, in the range of less than 20 atoms and it was measured both for ionic clusters [9] and for size selected neutral clusters deposited in rare gas matrix [10]. Nevertheless, the core *d* electrons play an important role. The screening induced by the *d* electrons is responsible for a global red-shift of the SPR frequency toward the near UV range as compared to the frequency expected from a pure jellium theory [1,6,7,11–13]. For gold, the threshold for interband transitions is much lower (of the order of 2 eV). This results in a stronger global red-shift of the SPR frequency and, in addition, a strong damping and broadening of the resonance band, as the particle size decreases [1,12,14,15]. For copper, the interband threshold is similar to that of gold, of the order of 2 eV. The SPR is in the same frequency range as gold, but experimentally this resonance band is much more damped and disappears at low sizes for particles of typically 2–3 nm in diameter (a few hundreds of atoms) depending on the observation conditions [16,17], e.g. on the dielectric constant of the matrix where the particles are embedded. This different behaviour of copper clusters [17] will be explained below.

To interpret the SPR band of noble metal nanoparticles, a classical approach, namely the Mie theory, is very often used. In this approach, the SPR band is simply calculated from the

E. Cottancin · G. Celep · J. Lermé · M. Pellarin
J.R. Huntzinger · J.L. Vialle · M. Broyer (✉)
Laboratoire de Spectrométrie Ionique et Moléculaire,
CNRS and Université Lyon 1, Bâtiment A. Kastler,
43, bd du 11 novembre 1918, 69622 Villeurbanne Cedex, France
E-mail: broyer@lasim.univ-lyon1.fr

frequency dependence of the bulk dielectric constant and the size of the nanoparticles is taken into account through the boundary conditions at the particle–matrix interface and the mean free path of the electrons. This approach is valid for large sizes typically for nanoparticles of diameter larger than 5 nm. However, this classical theory cannot be used to interpret the size dependence of the SPR band below 5 nm such as the blue-shift observed for gold clusters with decreasing sizes [12–14], as well as the complete damping of the SPR in small copper clusters.

On the other hand, a complete ab initio quantum treatment of the optical absorption of metal clusters can be performed [18,19], but it is presently limited to very small sizes and cannot be used to interpret the optical properties of clusters of the three noble metal clusters in the size range corresponding to diameter from 1 to 5 nm. For this purpose, we have recently developed a semi-quantal model [12,20] which is well adapted to this problem. Basically time-dependent local-density-approximation (TDLDA) calculations are carried out by using a model where the dynamical screening from the d electrons is taken into account through their contribution to the bulk dielectric constant.

The present paper is devoted to experimental and theoretical investigation of optical properties of noble metal clusters. The clusters of three metals, copper, silver and gold, in the size range 1–7 nm, have been produced by the same experimental technique, the deposition of preformed clusters in a transparent matrix. The recorded optical spectra are interpreted in the same framework of the semi-quantal model. The aim of the paper is to compare the three systems and to interpret completely the size dependence with the same theoretical model. The paper is divided into three main parts, the first concerns the experimental techniques, the second part is devoted to theoretical models and calculations and finally the obtained results are discussed in the third part.

2 Experiments

2.1 Sample preparation

Clusters are produced by a laser vaporization source described in previous papers [12,14,17]. In a small chamber under continuous flow of helium (a few tens of mbar), a rod of noble metal is vaporized by a frequency-doubled Nd–yttrium aluminium garnet (YAG) pulsed laser (532 nm). The so-formed metallic plasma, cooled by the inert gas, combines into clusters which expand with the inert gas in a nozzle before entering the high vacuum chamber (10^{-7} mbar) through a skimmer. The clusters are then co-deposited with the transparent alumina matrix (evaporated thanks to an electron gun) on various substrates whose kind depends on further measurements to be performed (Suprasil, carbon-coated microscope grids or silicon). The continuous helium flow allows a good stability of the cluster deposition rate. Moreover the helium pressure is a key to controlling the mean size of the free clusters, and thus, the size distribution in the samples. On the other hand, the metal volumic concentration inside the matrix is kept below 5% to minimize cluster coalescence. For that, cluster and matrix deposition rates are measured by two quartz balances which allow us to set the film thickness. The typical nanocomposite samples devoted to optical studies finally consist of a $1 \times 1\,\mathrm{cm}^2$ square suprasil substrate of 1 mm thickness coated with about 200 nm of alumina doped with noble metal clusters. Identical nanocomposite materials of lower thickness (15 nm) are deposited on carbon-coated grids for electron microscopy.

The substrate temperature may be varied. Usually clusters are deposited at room temperature. However, the substrate may be cooled by the circulation of liquid nitrogen to prevent coalescence during film growth. This was used to produce the smallest silver clusters (average diameter of 1.4 nm). The copper clusters deposited at room temperature have been found rapidly oxidized (Cu_2O). To prevent the oxidation process, the substrate was hold at a constant temperature of 400°C during the co-deposition. The X-ray photoelectron spectroscopy (XPS) was used to check the metallic character of copper nanoparticles [17]. We also found that the oxygen of the oxidized samples synthestized at room temperature may be removed by annealing under reducing atmosphere. We use typically one atmospheric pressure of H_2 (5%)–N_2 (95%). We obtained same results in both cases, but for the size evolution of optical properties of copper clusters, samples were prepared with substrate heated at 400°C during the co-deposition.

The cluster size distribution is measured by transmission electron microscopy (TEM). Figure 1 shows an example on silver clusters. Nanoparticles are almost spherical and randomly distributed. The dispersion of the size distribution is typically ±40% of the averaged size at half-maximum depending on the studied material and experimental conditions. For the discussion of optical measurements, we use the mean optical diameter $\Phi_{\mathrm{opt}} = <\Phi^3>^{1/3}$ which is slightly larger than the averaged size, the absorption cross-section being proportional to the particle volume.

Experiments were first performed on pure alumina samples without any metallic clusters in order to characterize the properties of alumina dielectric matrix. Alumina is found amorphous and the Rutherford back scattering (RBS) analysis reveals a slight overstoichiometry according to formula $Al_2O_{3.2}$. From thickness measurements, the matrix is found to have a porosity of about 40% as compared to crystalline alumina. The optical properties of the matrix are studied by ellipsometry, the dielectric constant is found slightly lower than for bulk alumina, typically $\varepsilon_{\mathrm{m}} \approx 2.7$ for our samples and $\varepsilon_{\mathrm{m}} \approx 3.1$ for the bulk.

2.2 Optical absorption spectra

Absorption measurements were performed with a double-beam Perkin-Elmer spectrophotometer on the thin films obtained by the method described above, in the spectral range 200–800 nm. Figure 2 shows selected examples of optical absorption spectra for gold and silver clusters. In both cases, a clear SPR emerges, but the two metals behave differently.

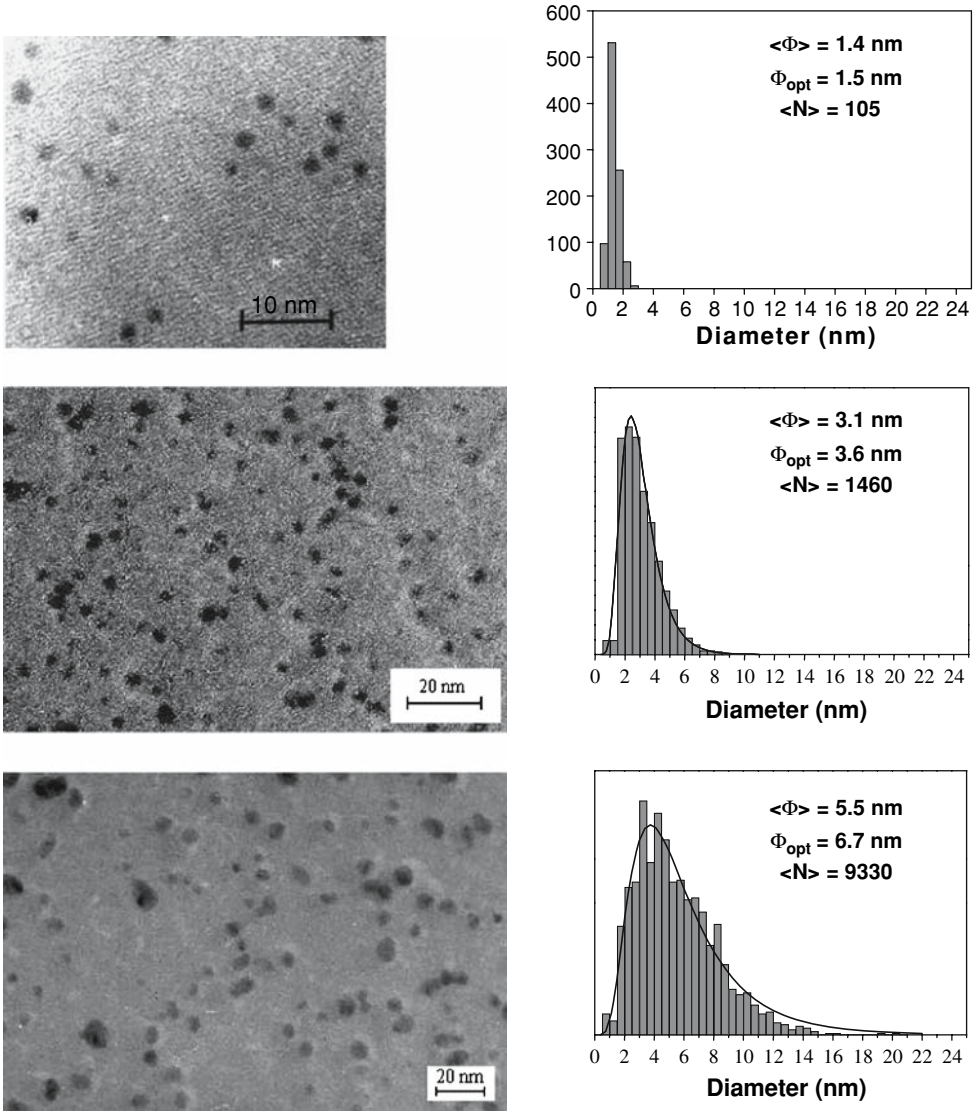

Fig. 1 *Left*: TEM micrographs of three samples of Ag_n clusters embedded in alumina. The first sample has been obtained by keeping the substrate temperature at 77 K, the other ones being elaborated at room temperature. *Right*: Size distribution of silver clusters deduced from the TEM micrographs. $<\Phi>$ and Φ_{opt} design the mean diameter and the optical diameter, respectively

In gold clusters, the SPR band occurs around 2.3–2.4 eV in the same spectral region than the threshold of the interband transitions (2 eV) which continue to increase in the UV range. Moreover a blue-shift and a damping of the resonance are observed when the cluster size decreases. This blue-shift is shown as a function of $1/R$ in Fig. 3.

In silver clusters, the SPR band occurs around 2.9–3.0 eV, well below the threshold of the interband transitions at 4 eV. Only a very small blue-shift of the resonance is measured when the cluster size decreases (Fig. 3).

Figure 4 shows the absorption spectra for three different sizes of copper clusters. The SPR band emerges quite hardly at about 2.15 eV from the steep increase of the interband transitions. Indeed in copper, the interband threshold is close to 2 eV (as in gold) but the corresponding absorption increases much more rapidly above 2 eV. In Fig. 4, the damping and the broadening of the SPR band, with decreasing sizes, is the most important feature of the experimental observations. In fact at very small sizes, the SPR band tends to vanish in the steep increase of the interband transitions. In the present experiments, it was not possible to produce clusters as small as 2 nm, but the complete damping of the resonance was observed by other authors for colloids [16]. In copper clusters, these damping and broadening of the SPR band are clearly the main size effects, rather than a strong blue-shift as in gold.

In conclusion of this experimental part, the differences in optical properties of the three metal noble clusters are quite striking, especially the influence of the size. We will demonstrate in the following that these differences can be interpreted by a semi-quantal model and discuss the limitations of the classical Mie theory.

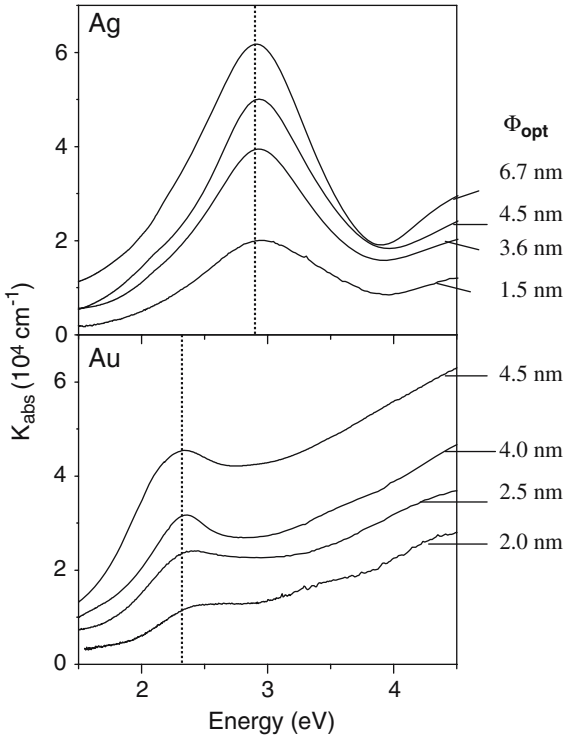

Fig. 2 Absorption coefficient versus energy of alumina embedded silver and gold clusters with various sizes. The smallest Ag_n and Au_n clusters are obtained by codepositon on cooled substrates

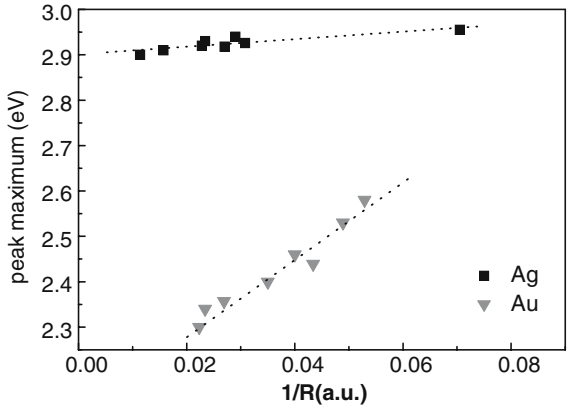

Fig. 3 Size evolution of the peak plasmon maximum obtained experimentally for gold and silver clusters embedded in an alumina matrix

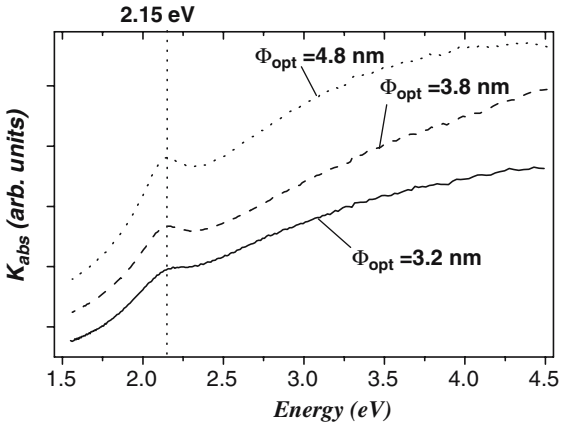

Fig. 4 Size evolution of the experimental absorption spectra for copper clusters versus energy

3 Theoretical models

3.1 Classical Mie theory

The classical Mie's theory for metal spheres (radius R) subject to an external electromagnetic field (wavelength λ) is the basic achievement for thoroughly understanding the evolution of the optical properties as a function of the ratio R/λ [21]. In cluster physics, the radii of the studied particles lie in the nanometer-size domain, corresponding to the dipolar- or quasi-static-approximation, where retardation effects can be neglected ($R/\lambda \ll 1$). For such small particles, the light extinction is exhausted by the dipolar absorption. Let us recall that the absorption cross-section of a matrix-embedded metallic sphere, in the dipolar approximation is given by

$$\sigma(\omega) = \frac{4\pi\omega}{c\varepsilon_{\mathrm{m}}^{1/2}} \mathrm{Im}[\alpha(\omega)], \tag{1}$$

where $\alpha(\omega)$ is the dynamical polarizability of the particle, c, the velocity of light, and, ε_{m}, the dielectric function of the matrix. In the case of a homogeneous sphere of dielectric function ε, $\alpha(\omega)$ is

$$\alpha(\omega) = \frac{\varepsilon - \varepsilon_{\mathrm{m}}}{\varepsilon + 2\varepsilon_{\mathrm{m}}} \varepsilon_{\mathrm{m}} R^3. \tag{2}$$

The dielectric function $\varepsilon(\omega)$ of the noble metal may be written as $\varepsilon = \varepsilon_1 + \mathrm{i}\varepsilon_2$ where ε_1 and ε_2 are, respectively, the real and imaginary parts of the metal dielectric function.

In noble metals, the contributions of s and d electrons to $\varepsilon(\omega)$ (respectively intraband and interband contributions) can be separated:

$$\varepsilon(\omega) = 1 + \chi^s(\omega) + \chi^d(\omega), \tag{3}$$

where $\chi^s(\omega)$ designs the Drude part of the dielectric susceptibility and $\chi^d(\omega)$the interband part (d electrons). The cross section $\sigma(\omega)$ has a resonant behaviour corresponding to the SPR which is obtained for $\varepsilon_1 = -2\varepsilon_{\mathrm{m}}$ if ε_2 has a low value. The resonance frequency ω_s is given at first approximation by

$$\omega_s = \frac{\omega_p}{\sqrt{2\varepsilon_m + \varepsilon_d^{\mathrm{re}}(\omega_s)}}, \tag{4}$$

where $\varepsilon_d(\omega) = 1 + \chi^d(\omega)$ is the interband part of the dielectric function, $\varepsilon_d^{\mathrm{re}}(\omega)$is the real part of $\varepsilon_d(\omega)$ and ω_p is the Drude bulk plasmon frequency; ω_p is given by

$$\omega_p = \sqrt{\frac{ne^2}{m_{\mathrm{e}}\varepsilon_0}}, \tag{5}$$

where n is the electronic density of s electrons and m_{e} their effective mass. $n^{-1} = 4\pi\, r_s^3/3$, r_s being the Wigner-Seitz (WS) radius.

Table 1 Electronic and optical properties of the three noble metals for atom and bulk

	Copper	Silver	Gold
Electronic structure	[Ar] $3d^{10}\,4s^1$	[Kr] $4d^{10}\,5s^1$	[Xe] $5d^{10}\,6s^1$
s–p resonance lines: $-s-p_{3/2}$	324.8 nm	328.1 nm	242.8 nm
	3.828 eV	3.779 eV	5.108 eV
$-s-p_{1/2}$	327.4 nm	338.3 nm	267.8 nm
	3.778 eV	3.666 eV	4.631 eV
Ionization potentials	7.726 eV	7.576 eV	9.225 eV
Interband threshold $(n-1)d \rightarrow$nsp	1.9 eV	3.85 eV	1.85 eV
	652 nm	322 nm	670 nm
Wigner–Seitz radius r_s	2.67 u.a.	3.02 a.u.	3.01 u.a.
Effective mass m_e	1.42 u.a.	1.03 u.a.	1.01 u.a.
Volumic plasmon energy $\hbar\omega_p$ for free s-electrons [including effective mass, Eq. (5)]	9.07 eV	8.85 eV	8.98 eV
d (Skin of ineffective screening)	3 a.u.	3.5 a.u.	3.5 a.u.

As shown in Table 1, the three noble metals have similar values of ω_p and according to formula (4), the energy of the SPR is mainly ruled by the real part of $\varepsilon_d(\omega_s)$. From the above formulas, it is clear also that no size effect, except the scaling factor R^3, is predicted in the absorption spectrum in the frame of Mie's theory in contrast with the experimental observations of Figs. 2, 3 and 4.

Figure 5 shows the real and imaginary parts of the dielectric function for the three noble metal clusters, respectively, Cu, Au and Ag. Clearly copper and gold have rather similar dielectric functions $\varepsilon_d(\omega)$. The interband thresholds are close to 2 eV in both cases (Table 1). The maximum of real part of $\varepsilon_d(\omega_s)$ is roughly the same, of the order of 11 (Fig. 5). The main difference lies in the steeper increase of the imaginary part of $\varepsilon_d(\omega_s)$ for copper, just above the interband threshold. In silver, the dielectric constant is completely different, with an interband threshold close to 4 eV and a much smaller value for the real part of $\varepsilon_d(\omega_s)$.

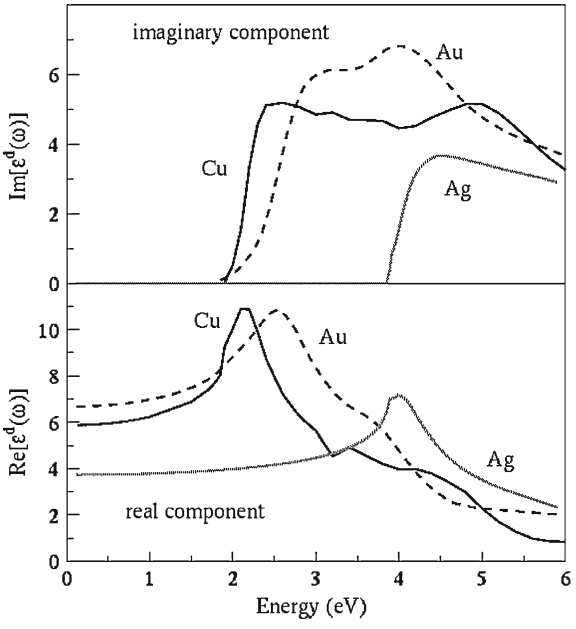

Fig. 5 Spectral dependence of the imaginary (*upper figure*) and real (*lower figure*) components of the complex dielectric functions $\varepsilon_d(\omega)$ corresponding to the interband transitions, for copper (*full line curves*), gold (*dashed line curves*) and silver (*grey line curves*). The interband thresholds are 1.9, 1.85 and 3.85 eV for Cu, Au and Ag, respectively

This explains the global features of the optical spectra of noble metal clusters as they are illustrated in Figs. 2, 3 and 4: the SPR lies around 2–2.5 eV for Cu and Au, in the region of interband transitions; while for Ag, the SPR occurs at around 2.9 eV and is well separated from the interband transition spectral range. This can be easily inferred from formula (4), considering the similar values of ω_p (Table 1) and taking into account the dielectric constant of the matrix ($\varepsilon_m \approx 2.7$ in our case).

In many theoretical investigations using the classical Mie's theory, this size dependence is *phenomenologically* introduced by invoking the so-called surface scattering-limited mean-free-path effect [1]. An R-dependent electron scattering rate is introduced in the Drude parameterization of the dielectric function associated to the conduction electrons:

$$\Gamma(R) = \Gamma_\infty + \frac{A v_F}{R}, \tag{6}$$

where v_F is the Fermi velocity and A is a model-dependent parameter.

The Drude dielectric function is then given by

$$\varepsilon^s(\omega) = 1 - \frac{\omega_p^2}{\omega[\omega + i\Gamma(R)]}. \tag{7}$$

With regard to the size effects, we can try to take them into account through the R-dependence of the electron scattering rate using formulas (6) and (7). Figure 6 shows the optical absorption cross-section calculated within this model for the three noble metals. The bulk dielectric functions are used in formula (1) and we take $A = 1$ in formulas (6) and (7). The Γ_∞ values are taken equal to 0.1 eV. The result is a red-shift for the SPR peak for gold and copper clusters in complete contradiction with the experimental results of Figs. 2, 3 and 4. In conclusion, the simple classical Mie theory cannot explain the size effects below a diameter of 6 nm. We really have to consider quantum finite-size effects.

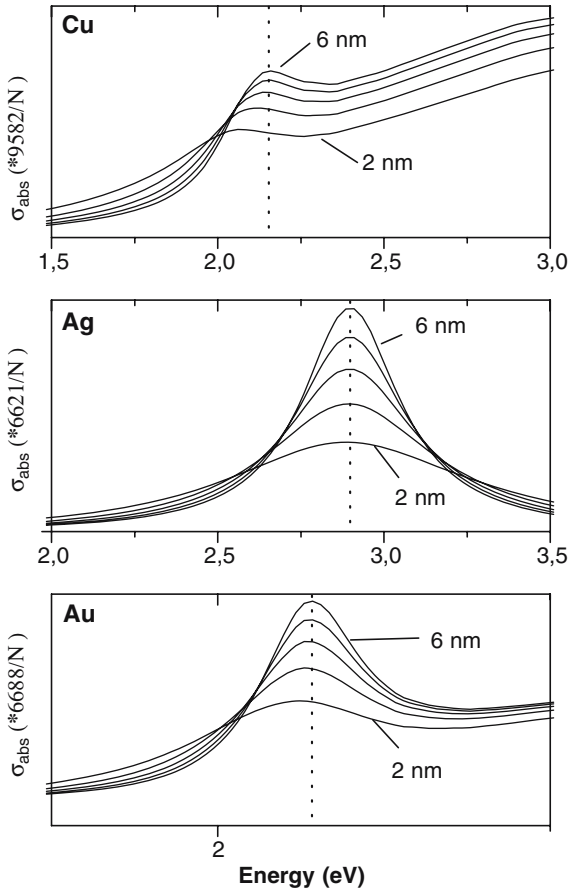

Fig. 6 Size evolution of the theoretical absorption cross-section versus energy within the classical Mie theory in the dipolar approximation, in taking into account the reduction of the mean free path in the particle, for gold, silver and copper clusters embedded in porous alumina ($\varepsilon_{\mathrm{m}} \approx 2.7$)

3.2 Semi-quantal theory

For obvious computational constraints ab initio methods cannot be carried out for large clusters, and are restricted to small sizes (a few tens of atoms at the maximum) and/or low-Z elements [19,22]. This is especially true for noble metals where orbitals of both s and d electrons have to be considered in the calculations in contrast with alkali clusters.

In this respect, as long as large particles are involved, structureless jellium-type model approaches seem to be quite appropriate and reasonable for investigating mean size trends over large size domains, as well as for comparison purpose between various metallic species. The calculations made on large noble metal clusters are based on the TDLDA formalism and the density functional theory (DFT), within a structureless jellium-type model including – phenomenologically – the absorption and screening properties of both the ionic-core background and the surrounding matrix [20]. This model has been detailed and discussed in previous papers, so we recall only the main ingredients here.

The conduction electrons corresponding to the s–p band, responsible for the collective surface plasmon excitation, and underlying most of the (quantum) finite-size effects, are quantum mechanically treated. The ionic background including the screening by the d electrons is phenomenologically described by: (1) a step-walled homogeneous spherical charge distribution (*jellium*) of radius $R = r_s N^{1/3}$ (r_s is the WS radius per conduction electron in the bulk), and, (2) a homogeneous dielectric medium [complex dielectric function $\varepsilon_d(\omega)$, corresponding to the interband transitions, assumed to be bulk-like] extending up to $R_c = R - d$ where d is the skin thickness of ineffective ion polarizability (ineffective screening). This last ingredient, which is of main importance for explaining the finite-size effects in noble metal clusters, as compared to alkali elements, deserves to be commented.

This skin of vanishing polarizability was introduced by Liebsch [23] in the context of electron energy loss at metal surfaces, and applied early to rare-gas matrix-embedded Ag_{N-}clusters within a classical Mie-like approach involving concentric nested dielectric media [10]. This surface property, subsequently discussed by several authors [13,24,25] is thought to be related to both the spatial localization of the d-electron wave functions relative to the WS radius [24] and the change of the effective polarizability of the ionic-cores depending on the embedding medium or local environment [25]. Strictly speaking the thickness d has to be considered as a free phenomenological parameter. In view of the approximation consisting in replacing the discrete ionic structure by homogeneous step-walled jellium and dielectric medium, a rigorous prescription for setting its value cannot be defined. In this work, the value has been set in order to reproduce the experimental finite-size effects observed in free Ag_N^+ clusters [9]. This procedure leads to the value $d \approx 3.5$ a.u., of the order of the WS radius of silver metal ($r_{\mathrm{s}} = 3.02$ a.u.). Calculations involving nonlocal pseudopotentials show that the long-range part of the nd-wave functions is quite similar for Ag and Au atoms. Since, moreover, both metals have almost identical r_{s} values, the same phenomenological parameter d has been also selected for gold. The value $d = 3$ a.u., slightly lower than that chosen for Ag and Au particles, has been taken for Cu_N particles, in assuming the rough scaling law $d(\mathrm{Cu}) \approx d(\mathrm{Ag, Au})[r_{\mathrm{s}}(\mathrm{Cu})/r_{\mathrm{s}}(\mathrm{Ag, Au})]$ (smaller ion-core size for copper). Let us stress that both values, $d = 3$ a.u. and $d = 3.5$ a.u., yield almost identical absorption spectra. The complex dielectric function $\varepsilon_d(\omega)$, corresponding to the interband transitions, is carefully extracted from the experimental complex dielectric function $\varepsilon(\omega)$ of the bulk. This is done by a Kramers Kronig analysis after subtracting the s electron contribution $\varepsilon_s(\omega)[\varepsilon(\omega) = \varepsilon_s(\omega) + \varepsilon_d(\omega) - 1]$ in the imaginary component, $\varepsilon_s(\omega)$ being calculated by the Drude formula.

To take into account the influence of the local porosity of the matrix, a vacuum rind of thickness d_{m} is introduced in the model in order to mimic the spherically averaged local porosity. We use $d_{\mathrm{m}} = 2$ a.u, as in our previous papers [12,14,17]. The value $d_{\mathrm{m}} = 2$ a.u. has been selected in fitting the model predictions with our experimental data on our embedded Ag_N particles. Since the composite metal/alumina porous films have been elaborated under the same experimental

deposition conditions for the three noble metals, except for the substrate heating in the case of copper, the same value has been taken for all the systems. Let us remark that the effective parameters d and d_m have been independently determined. The mixed classical/quantal model involves thus three nested geometric interfaces, located at $r = R - d$, $r = R$ (jellium radius) and $r = R + d_m$, but two "background"-dielectric interfaces ($\varepsilon_b \equiv \varepsilon_d$ for $r < R - d$, $\varepsilon_b = 1$ between $R - d$ and $R + d_m$, and $\varepsilon_b \equiv \varepsilon_m$for $r > R + d_m$). In a pure classical Mie-like model, the conduction-electron contribution ε_s has to be added to ε_b in the radial range r<R.

We discuss now the last relevant free parameter of the model, as well as the "problem" of the resonance band width. In the TDLDA formalism [26,27], the evaluation of Green's function $G(\mathbf{r}, \mathbf{r}', E) =< \mathbf{r}[H - E - i\delta]^{-1}\mathbf{r}' >$ (H is the single-particle Kohn–Sham Hamiltonian of the DFT), that is involved for calculating the independent-electron density–density correlation function $\chi_0(\mathbf{r}, \mathbf{r}', E)$, requires the use of a finite value for the infinitesimal δ-parameter. Actually, δ acts as an *effective* numerical smoothing parameter, which may be used to mimic crudely the line broadening arising from physical effects that are disregarded in such a model, as for instance the vibrational spectrum of the ionic lattice or the removal of the electron level-degeneracy resulting from the discrete structure, surface roughness or thermal shape fluctuations [28]. In the present model, this amounts – in a rough picture – to attributing an intrinsic width 2δ to each bound–bound one-electron excitation line (Lorentzian-shaped peak). Therefore, in the absence of Landau damping [29], the minimum plasmon band width is equal to 2δ. For silver, this "asymptotic" value is obtained for the largest calculated sizes. On the other hand, in the case of gold and copper, the absorption cross-section does not depend strongly on the selected δ-value because of the large interband-induced broadening, except for very small sizes which exhibit a more conspicuous fragmentation pattern. The value δ=100 meV has been used in the calculations reported in this paper.

For simple metals, as well as for silver where the interband threshold is much higher than the SPR, a large part of the plasmon band broadening is exhausted by the so-called Landau damping [29], namely the coupling of the collective dipolar excitation with energetically close individual electron–hole (e–h) excitations. This yields a "fragmented" band pattern exhibiting several distinct lines. In the large size range the e–h excitation spectrum is strongly congested, and the various lines merge into a single Lorentzian-shaped resonance band, whose width evolves according to formula (6). This mechanism has been described early [30] in the case of metal particles, and the scaling law has been supported by TDLDA jellium calculations involving a very large size range [31]. In copper and gold clusters, the strong broadening of the plasmon band stems mainly from the coupling with the interband transitions, their threshold occurring just below the SPR spectral region.

The calculated sizes shown in the following are electronic closed shells (typically 138, 440, 832, 1,314, 2,048, etc.). This allows an easier and faster convergence for the iterative solving of the self-consistent ground-state Kohn–Sham equations, which is required in the TDLDA formalism.

The semi-quantal model used above could be improved for handling small and medium cluster sizes in using some features of the polarizable core approach introduced by Serra and Rubio [32], but at the price of much more lengthy computational times.

In their approach, the discrete cluster structure is retained. The dipole moments $\mathbf{p}_j = \alpha_j(\omega)\mathbf{E}_j$ at each ionic site j, which are responsible for the valence electron interaction screening, are determined – within a self-consistent scheme – in calculating the local electric field $\mathbf{E}_j$ near each site. From the discrete dipole distribution, the electric potential produced by the ionic background is thus obtained. Then the time-dependent conduction electron density $\delta\rho(\mathbf{r}, t)$ is calculated thanks to the central TDLDA-formula linking $\delta\rho(\mathbf{r}, t)$ and the total effective potential $\Phi_{tot}(\mathbf{r}, t)$ through the independent-electron density–density correlation function $\chi_0(\mathbf{r}, \mathbf{r}', t)$. The input data of this approach are thus the ion polarizabilities $\alpha_j(\omega)$ which are assumed to depend only on the local valence electron density near the site j and is computed in an embedded-atom approximation. In practice, since the valence electron density is rather flat inside the particle and decreases abruptly at the surface, $\alpha_j(\omega)$ is taken, either as the free ion polarizability (surface ions), or as the fully embedded-core polarizability corresponding to the bulk density (inner ions). Actually this prescription amounts to introducing the surface skin of ineffective polarizability of thickness d. At this stage, the "microscopic" approach of Rubio [32] is nothing else as the "discrete" version of the "structureless" jellium-type semi-quantal model of Ref. [20]: the smooth polarization field induced by the background dielectric function $\varepsilon_d(\omega)$ is replaced by the field created by a distribution of point-like dipoles. Clearly, such a model refinement provides to some extent physical support to the phenomenological two-region dielectric model used in this paper. However, it is only applicable for small or medium cluster sizes, containing up to a few hundreds atoms because it requires for each size a specific ionic geometry. Therefore, it is not adapted to investigate finite-size effects over a large size range.

4 Comparison between experimental results and semi-quantal calculations

Figure 7 shows the comparison between experiment and semi-quantal theory for the size evolution of the peak plasmon in alumina-embedded Au_n and Ag_n clusters. Calculations are performed using for $\varepsilon_m(\omega)$ the tabulated bulk value in the visible range ($\varepsilon_m \approx 3.1$) or the data of ellipsometry measurements for our porous alumina films ($\varepsilon_m \approx 2.7$). The theoretical calculations well reproduce the experimental trends, namely the strong blue-shift of the SPR for gold and a very small blue-shift for silver, as the cluster size decreases. This blue-shift is mainly due to the skin thickness d of ineffective screening of the d electrons which results in a blue-shift of the SPR that is all the more important that the sizes are

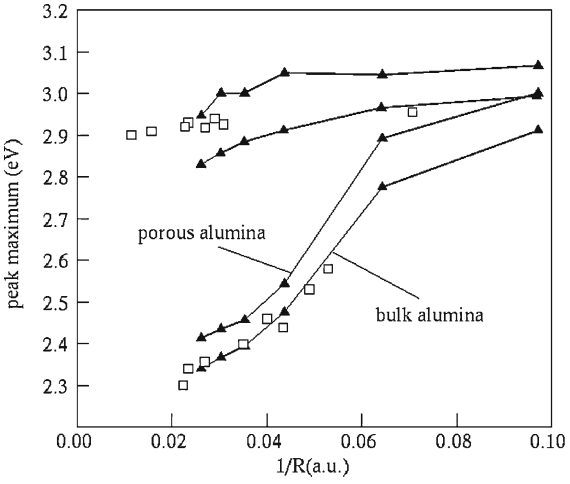

Fig. 7 Size evolution of the peak plasmon maximum for alumina-embedded Au_n (*lower curves*) and Ag_n (*upper curves*)clusters. The open square symbols are the experimental results. The "effective" radius characterizing each sample has been identified with the "optical radius" defined as $R_{\mathrm{opt}} = \sqrt[3]{< R^3 >}$. The *black triangles* are the theoretical predictions obtained in the framework of the mixed classical/quantal model, involving an inner skin of vanishing ionic-core polarizability (thickness $d = 3.5$ a.u.) and an outer vacuum rind mimicking the local porosity at the metal–matrix interface (thickness $d_{\mathrm{m}} = 2$ a.u.). Two hypotheses have been considered with regard to the dielectric function characterizing the matrix beyond the vacuum rind, i.e. for $r > R + d_{\mathrm{m}}$. The first model involves the bulk–alumina dielectric function [37], and the second the porous–alumina dielectric function determined by ellipsometry measurements

small. This blue-shift competes with the red-shift associated to the spillout of the *s* electrons. This spillout phenomenon corresponds to the escape of the electronic cloud outside the jellium boundary and is a pure quantum effect. In gold the blue-shift is predominant as compared to the spillout red-shift. In silver both are close to be compensated, inducing a rough quenching of the size effects. This different behaviour of gold and silver clusters is easy to understand because the real part of ε_d (which measures the screening) is much smaller in silver (of the order of 4) than in gold (of the order of 11), as illustrated in Fig. 5. The agreement between theory and experiment is very good. The use for ε_{m} of the bulk or of the measured value does not change the global agreement, the experimental results being located in between. The small change of ε_{m} induces only a global shift of the SPR. Indeed, since part of the porosity is already taken into account by the vacuum rind d_{m}, it is difficult to decide what the best value for ε_{m} is. That illustrates the limits of our model of a vacuum rind to account for the porosity.

Let us now compare gold and copper clusters. The dielectric functions due to interband transitions are similar in both cases (Fig. 5). The Mie theory leads also to rather similar absorption spectra as illustrated in Fig. 6. Experimentally (Fig. 4) the behaviour for small sizes is completely different. For copper, we hardly observe a blue-shift of the resonance as the size decreases, and mainly a strong damping and a broadening. This result cannot be interpreted by the Mie theory which predicts a red-shift when the size decreases (Fig. 6). Figure 8 shows the comparison between experimental results and semi-quantal theory. The theoretical curves in this figure show that the resonance band (SPR) gradually vanishes in the rising edge of the interband transitions as the size decreases. Qualitatively, and also quantitatively (except the slight blue-shift which is less clear in the experiment), the calculations are in very good agreement with the experiment. As a matter of fact, a strict comparison with the experimental spectra would require taking into account the size, shape and local environment distributions for each sample. Therefore, considering the approximations done to interpret the experiments (single size and perfect spherical shape and symmetry), the agreement is extremely good, and we obtain in copper clusters a complete description of the progressive emergence of the SPR from the rising edge of the interband transitions as the particle size increases. In gold, the SPR remains apparent even for very small sizes (Fig. 2, 9), the interband transitions being much less steep (Fig. 5), at least in the threshold region.

In conclusion of this paragraph, Fig. 9 shows the comparison between experiments and theoretical semi-quantal calculations for the three noble metal clusters, silver, gold and copper. The agreement is excellent for the positions of

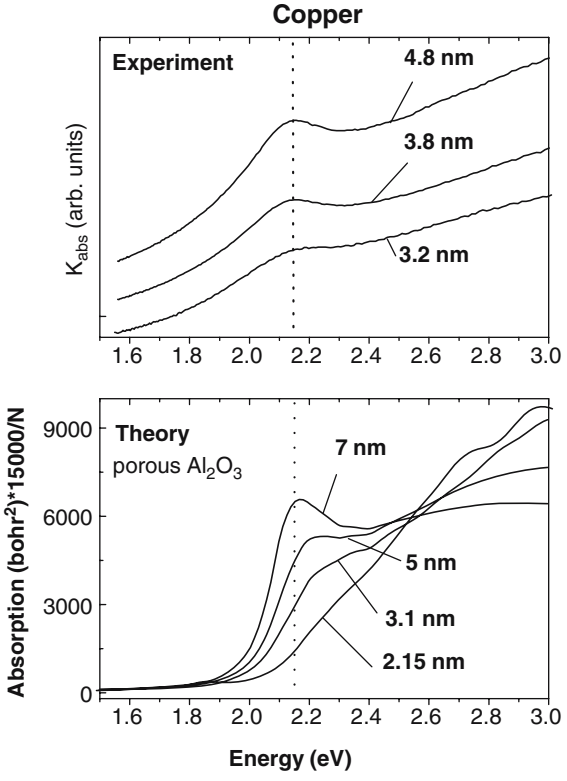

Fig. 8 Comparison between experimental spectra and absorption cross-sections calculated with the semi-quantal theory for different sizes of copper clusters. To normalize the curves corresponding to different sizes, the theoretical data have been multiplied the volumic ratio $15,000/N$ (N being the number of atoms). The measured dielectric function of porous alumina deposited on warmed substrate is used ($\varepsilon_{\mathrm{m}} \approx 2.75$)

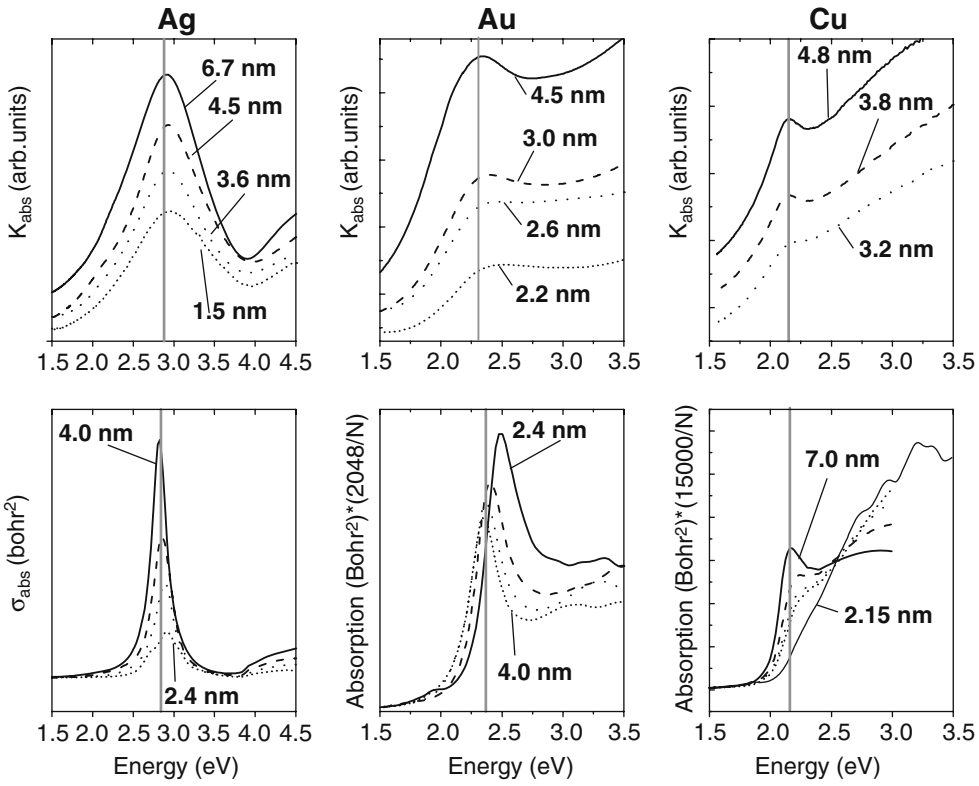

Fig. 9 Size evolution of the experimental absorption spectra and of the theoretical ones obtained in the semi-quantal model (see the text) for the three noble metals: gold, silver and copper

the resonance peaks and for the size evolution. As the size decreases, we obtain a small blue-shift for silver clusters, a pronounced blue-shift for gold and a gradual disappearance of the SPR in the rising edge of the interband transitions for copper. In the model used for calculations the main parameter is the skin d of ineffective screening by the d electrons. This parameter d is not arbitrary. As explained above, it was already introduced in the context of electron energy loss at metal surfaces and has been fitted independently from experimental measurements on free ionic silver clusters. We use the same d values for the three noble metals except for a reasonable scaling factor involving the Wigner size radius.

We therefore obtain a complete description of the optical properties of the free noble metal clusters in the size domain ranging from 1.5 to 10 nm (in diameter). Above 10 nm, the quantum size effects are negligible and the Mie theory is well adapted.

Concerning the resonance band width, it is worth emphasizing that a perfect agreement with the experimental spectra cannot be achieved because a large part of the experimental band width originates from inhomogeneous effects, namely the size, shape and local environment (interface and local porosity) distributions in each sample. As expected, the experimental bandwidth is systematically larger than the theoretical ones in Fig. 9, except for very small sizes of Cu an Au clusters (2–3 nm), where the broadening is mainly due to the coupling with the interband transitions.

5 Conclusion

The size evolution of the optical properties of the three noble metal clusters have been investigated both theoretically and experimentally. General trends can be deduced from this study. On a very general point of view, the optical properties of copper and gold clusters appear rather similar. This is mainly due to the position of the d band as compared to the s–p band which is rather similar in both cases with an interband threshold close to 2 eV. This is not the case for other properties. For example, if we consider the atomic properties (table 1) like the ionization potentials (IP) and the s–p resonance lines of copper and silver are rather similar. Due to relativistic effects, the IP and s–p resonance lines of gold have significantly higher energy. The geometric structures of gold clusters are also very different, with planar structures up to 12 atoms for anions while copper and silver clusters have compact structures [33,34]. This is not surprising, the geometric structure of clusters being mainly driven from the properties of the atomic orbitals of electrons responsible for the bonding. The optical properties, in particular for clusters of typically more than 100 atoms (more than 1.5 nm in diameter), are mainly related for noble metals to the relative positions of s and d bands, as already noted.

The semi-quantal calculations are, to our knowledge, the best compromise between completely ab initio methods limited to relatively small sizes and completely classical

calculations which cannot take into account the quantum size effects. We have shown that these semi-quantal calculations, with a very limited number of semi-empirical parameters, are able to predict the optical properties of the three noble metals in a size range from 1.5 to 10 nm in diameter.

It remains that the comparison between experiments and theory is limited by the size and shape distributions of the sample. To improve this situation, we have recently demonstrated the possibility to observe directly the optical absorption of single noble metal nanoparticles [35] by a new ultra sensitive optical microscope. This kind of experiment opens the route to a very precise comparison with the theory and also to a new field concerning the interaction with the environment or the interaction between small nanoparticles. We have also developed a static quadrupole deviator for the deposition of size selected clusters [36]. This system coupled with the new ultra sensitive microscope will allow undertaking this new program.

Acknowledgements Michel Broyer wants to specially acknowledge Jean Paul Malrieu for very helpful and encouraging discussions during 20 years of research on cluster physics. Jean Paul strongly encourages him to approach this quite complex field. In particular, the physics of transition metal clusters was a real challenge. We think that our present work on noble metal clusters contains all the main ingredients that Jean Paul tries to teach us during his very successful career: the interest for studying complex systems, the importance of performing complicated calculations with the best state of art available and finally the necessity to analyse the calculations in order to extract the key physical content. In this respect, we think the optical properties of noble metal clusters represent some kind of text book example since they need very refined calculations and they may be interpreted by simple physical pictures. Moreover, the colours of these materials have fascinated scientists and artists since the beginning of the civilization. We want also to thank Bruno Palpant and Melanie Gaudry who have done their Phd thesis on part of the present work and Laurent Arnaud for the TEM measurements. Brigitte Prevel has also participated to the beginning of this work. The experiments described in this paper have been done in the frame of the Lyon cluster facility. One of us (Michel Broyer) was supported by the Institut Universitaire de France.

References

1. Kreibig U, Vollmer M (1995) Optical properties of metal clusters, Springer, Berlin, Heidelberg, New York
2. Klar T, Perner M, Grosse S, v. Plessen G, Spirkl W, Feldman J (1998) Phys Rev Lett 80:4249
3. Ditlbacher H, Krenn JR, Schider G, Leitner A, Aussenegg FR (2002) Appl Phys Lett 81:1762
4. Boyer D, Tamarat P, Maali A, Lounis B, Orrit M (2002) Science 297:1160
5. Cogswell CG, Hamilton DK, Sheppard CJR, Microsc J (1992) 165:103
6. Heer WAD (1993) Rev Mod Phys 65:611
7. Wang CRC, Pollack S, Kappes MM (1990) Chem Phys Lett 166:26
8. Blanc J, Bonacic-Koutecky V, Broyer M, Chevaleyre J, Dugourd P, Koutecky J, Scheuch C, Wolf JP, Wöste L (1992) J Chem Phys 96:1793
9. Tiggesbäumker J, Köller L, Meiwes-Broer KH, Liebsch A (1993) Phys Rev A 48:R1749
10. Fedrigo S, Harbich W, Buttet J (1993) Phys Rev B 47:10706
11. Liebsch A (1993) Phys Rev Let 71:145
12. Palpant B, Prével B, Lermé J, Cottancin E, Pellarin M, Treilleux M, Pérez A, Vialle JL, Broyer M (1998) Phys Rev B 53:1963
13. Lermé J, Palpant B, Prével B, Pellarin M, Treilleux M, Pérez A, Vialle JL, Broyer M (1998) Phys Rev Lett 80:5105
14. Gaudry M, Lermé J, Cottancin E, Pellarin M, Vialle J, Broyer M, Prével B, Treilleux M, Mélinon P (2001) Phys Rev B 64:085407
15. Alvarez MM, Khoury JT, Schaaff TG, Shafigullin MN, Vezmar I, Whetten RL (1997) J Phys Chem B 101:3706
16. Lisiecki I, Pileni MP (1995) J Phys Chem 99:5077
17. Celep G, Cottancin E, Lermé J, Pellarin M, Arnaud L, Huntzinger JR, Vialle JL, Broyer M, Palpant B, Boisron O, Mélinon P (2004) Phys Rev B 70:165409
18. Bonacic-Koutecky V, Fantucci P, Koutecky J (1991) Chem Rev 91:1035
19. Bonacic-Koutecky V, Veyret V, Mitric R (2001) J Chem Phys 115:10450
20. Lermé J (2000) Eur Phys J D 10:265
21. Mie G (1908) Ann Phys 25:377
22. Blase X, Ordejon P (2004) Phys Rev B 69:085111
23. Liebsch A (1993) Phys Rev B 48:11317
24. Krésin VV (1995) Phys Rev B 51:1844
25. Serra L, Rubio A (1997) Z Phys D 40:262
26. Stott MJ, Zaremba E (1980) Phys Rev A 21:12
27. Zangwill A, Soven P (1980) Phys Rev A 21:1561
28. Moseler M, Häkkinen H, Landman U (2001) Phys Rev Lett 87:053401
29. Yannouleas C, Broglia RA (1991) Phys Rev A 44:5793
30. Kawabata A, Kubo R (1996) J Phys Soc Jpn 21:1765
31. Yannouleas C (1998) Phys Rev B 58:6748
32. Serra L, Rubio A (1997) Phys Rev Lett 78:1428
33. Furche F, Ahlrichs R, Weis P, Jacob C, Gilb S, Bierweiler T, Kappes M (2002) J Chem Phys 117:6982
34. Häkkinen H, Yoon B, Landman U, Li X, Zhai HJ, Wang LS (2003) J Phys Chem A 107:6168
35. Arbouet A, Chistofilos D, Fatti ND, Vallée F, Huntzinger JR, Arnaud L, Billaud P, Broyer M (2004) Phys Rev Lett 93:127401
36. Alayan R, Arnaud L, Bourgey A, Broyer M, Cottancin E, Huntzinger JR, Lermé J, Vialleb JL, Broyer M, Guiraud G (2004) Rev Sci Instrum 75:2461
37. Palik ED (1985/1991) Handbook of optical constants of solids, Academic, New York